Peer-reviewed version available at *Catalysts* **2018**, *8*, 374; doi:10.3390/catal8090374

Communication

Enhancement photocatalytic activity of the heterojunction of two-dimensional hybrid semiconductors ZnO/V_2O_5

Juan Aliaga[1], Nasla Cifuentes[1], Guillermo González[3,4] Clivia Sotomayor-Torres[5,6] and Eglantina Benavente[1,2]*

1 Universidad Tecnológica Metropolitana, P.O. Box 9845, Santiago, Chile; nasla.cifuentes@utem.cl.
2 Programa Institucional de Fomento a la I+D+i, Universidad Tecnológica Metropolitana, Ignacio Valdivieso 2409, P.O. Box 8940577, San Joaquín, Santiago, Chile; jaliaga@utem.cl.
3 Universidad de Chile, P.O. Box 653, Santiago, Chile; ggonzale@uchile.cl
4 Center for the Development of Nanoscience and Nanotechnology, CEDENNA, Av. Ecuador 3493, Santiago, Chile.
5 Catalan Institute of Nanoscience and Nanotechnology (ICN2), CSIC and BIST, Campus UAB Bellaterra, 08193 Barcelona, Spain; clivia.sotomayor@icn2.cat.
6 ICREA, Pg. Lluís Companys 23, 08010 Barcelona, Spain

* Correspondence: ebenaven@utem.cl; Tel.: +56-227877109

Abstract:

In this work, we report the fabrication of the new heterojunction of two 2D hybrid layered semiconductors, ZnO(stearic acid)/V_2O_5(hexadecylamine), and its behavior in the degradation of aqueous methylene blue under visible light irradiation. The optimal photocatalyst efficiency, reached at a ZnO(stearic acid)/ V_2O_5(hexadecylamine) ratio of 1:0.25, results to be about six times higher than that of pristine zinc oxide. Reusability test shows that after three photocatalysis cycles no significant changes in neither the dye degradation efficiency loss nor photocatalyst structure occur. Visible light photocatalytic performance observed indicates there is synergetic effect between both 2D nanocomposites used in the heterojunction. The visible light absorption enhancement promoted by the narrower bandgap V_2O_5 based components; an increased photo generated charge separation favored by extensive interface area; and abundance of hydrophobic sites for dye adsorption appear as probable causes of the improved photocatalytic efficiency in this hybrid semiconductors heterojunction. Estimated band-edge positions for both conduction and valence band of semiconductors together with experiments using specific radical scavengers allow a plausible photodegradation mechanism.

Keywords: Photocatalysis, heterojunction, two dimensional semiconductor, ZnO, V_2O_5, Methylene blue degradation

Peer-reviewed version available at Catalysts 2018, 8, 374; doi:10.3390/catal8090374

1. Introduction

The use of solar energy is increasingly needed to address many of the growing energy and environmental problems facing humanity. Processes like the production of clean fuels from abundant natural resources or the degradation of pollutants based on sunlight-driven reactions, catalyzed by nano-structured semiconducting metal oxides, have received much attention during the last decades [1,2]. These are heterogeneous processes where the role of the photocatalyst is similar to that of the electrodes in electrolysis in the sense of promoting, separately but simultaneously, a redox reactions pair with given substrates adsorbed on its surface. The conversion of radiation energy into chemical energy mainly depends on both, the ability of the semiconductor for creating effective redox centers on its surface and the tendency of the substrate to be adsorbed nears these sites. The photoinduced creation of active redox sites starts with the excitation of electrons from the valence band of the semiconductor to the conduction one by absorption of light with energy equal to or greater than its band-gap generating electron-hole pairs (e-/h+). After the separation of these charge pairs, mediated by internal or external electric fields, electrons and holes migrate to spatially separated places at the interface between the particle with its environment, where they can respectively reduce or oxidize suitable substrates [3, 4].

The use of wide band, high valence metal oxides such as TiO_2 and more recently ZnO as photocatalysts has been extensively studied. The electronic structure of these semiconductors, particularly the position of their valence band edge (about 3.0 eV vs NHE) give then interesting photochemical activity and high resistance to photocorrosion in water solutions; this together with their generally non-toxicity and low cost make them promissory for large-scale environmental remediation applications[5,6]. However, their photocatalytic efficiency, and thus their large-scale applications, is affected by some of their intrinsic properties. Among them, a narrow absorption window that excludes much of the solar spectrum; high recombination rates of light-induced charges leading to poor quantum yields; and relatively high hydrophilic surfaces unfavorable for the adsorption of non-polar substrates [7]. Much efforts are been investing in solving these hindrances. Although most reports on this subject concern TiO_2, during the last years ZnO a n-type semiconductor with direct band gap (3.37 eV) and high exciton binding energy (60 meV), has receiving increasing attention [8,9]. The role of the morphology of ZnO nanostructures on its photocatalytic performance in the decomposition of organic molecules is being intensively studied [10, 11]. In general anisotropic micro/nano-structures are more efficient because together with promoting charge carrier generation rate (nano-scale), allow higher mean-path-length of the photoinduced charges. This among others reduces charge-carriers recombination, promotes effective charge separation, and makes more facile the migration of charge carriers to their reaction sites. Similar effect have been attained by loading noble metals such as Au, Ag, Pd and Pt as co-catalysts [12-14] and by the formation of ZnO heterojunctions with other semiconductors like TiO_2, $BiVO_4$, Ag_2O or Cu_2O [14-18]. Numerous attempts to extend the light absorption window of ZnO -naturally centered in the ultraviolet- towards lower energies have been also reported [19]. ZnO sensitization by heterojunction with (relatively minor amount of) a second lower band gap semiconductors like CdS and WO_3 [20,21] has demonstrated to effectively improve its photocatalytic activity under visible light. In these systems the main absorber mainly is the secondary semiconductor while the role of ZnO is principally limited to the charge curriers transport. That notwithstanding, some interesting approaches to directly improve ZnO visible-light absorption have been also attempted; namely by creating electronic levels within the ZnO band gap, by metal or non-metal doping, or surface modification via organic materials graphting [22-25]. Most attempts to improve the photocatalysis of organic contaminants optimizing the adsorption of the substrates upon the photocatalyst mainly concern to the increment of its specific surface area, so the utilization of 2D layered materials that have larger specific surface areas, a great number of active sites on the surface and superior electron mobility that facilitate the transfer and separation of photogenerated electrons and holes, is a good

strategy for constructing effective photocatalyst [26,27]. Approach considering additives to increase the hydrophobicity of the semiconductor surface, like the use of surfactants reported for TiO_2 are in general scarce for ZnO [25,28-32]. In this direction we recently developed laminar hybrid 2D ZnO-organic nanocomposites in which the surfactant grafted to the inorganic matrix significantly improves the photocatalytic process and we evaluate your photocatalytic activity combined with VOx-NTs in different mixing ratios [33]. Studies, for example, Yin et al. reported of enhanced photocatalytic degradation of methylene blue (MB) in V_2O_5/ZnO heteronanorods [34], Zou et al. reported of enhanced photocatalytic activity in decomposition of chlorophenol in ZnO/V_2O_5 core-shell nanostructures [35] and Aslam et al. reported of enhanced photocatalytic activity in decomposition of nitrophenol with ZnO/V_2O_5 nanocomposites[36]. The capability of V_2O_5 to sensitize the ZnO nanocomposite makes the system a very attractive and new material for studied of heterogeneous photocatalysis.

In this work we evaluated the photocatalytic activity of the organic-inorganic laminar ZnO(stearic acid) with a band gap (Eg) of 3.28 eV combined with organic-inorganic hybrid V_2O_5/(hexadecylamine), (Eg = 3.28) in the degradation of aqueous methylene blue solution in visible light. In addition, we have realized various combinations with V_2O_5 and V_2O_5-xerogel to investigate the photocatalytic activity. The blend of both organic-inorganic hybrid semiconductors 2D/2D produces the expected synergy improving the degradation of the dye selected as organic contaminant model. Furthermore, tentative mechanism was also discussed based on the active species trapping experiments and estimated band edge positions.

2. Results and Discussion

The XRD pattern of synthesized nanocomposites are shown in Figure 1. The lamellar nature ZnO(stearic acid) (ZnO(SA)) in Figure 1(a) and V_2O_5(hexadecylamine) (V_2O_5(HDA)) in Figure 1(b) constituted of single nanosheets of semiconductor sandwiched between self-assembled of surfactants are confirmed by the X-ray diffraction patterns, which display low angle reflections, characteristic of well-ordered laminar arrangements 2D, according to the positions of the 00l reflections in the diffraction pattern, the interlayer distances along the c-axis corresponding to the first peak in the low angle XRD pattern, which correlate well with the molecular lengths of corresponding carboxylic acid and alkylamine, previously reported [37,38]. In figure 1(a) also shows the reflections that indicate the inorganic moiety corresponding to ZnO single phase with the wurtzite structure (JCPDS 36-1451). Figure 1(c) shows the XRD patterns of heterojunction ZnO(SA)/V_2O_5(HDA), two types of phases were detected, one type of phase well defined of ZnO(SA) and 001 plane to V_2O_5(HDA), reveal the formation of layered structure with both composites. In this XRD pattern, no other possible impurities were detected which suggested that nanocomposites ZnO(SA) and V_2O_5(HDA) remains unaltered.

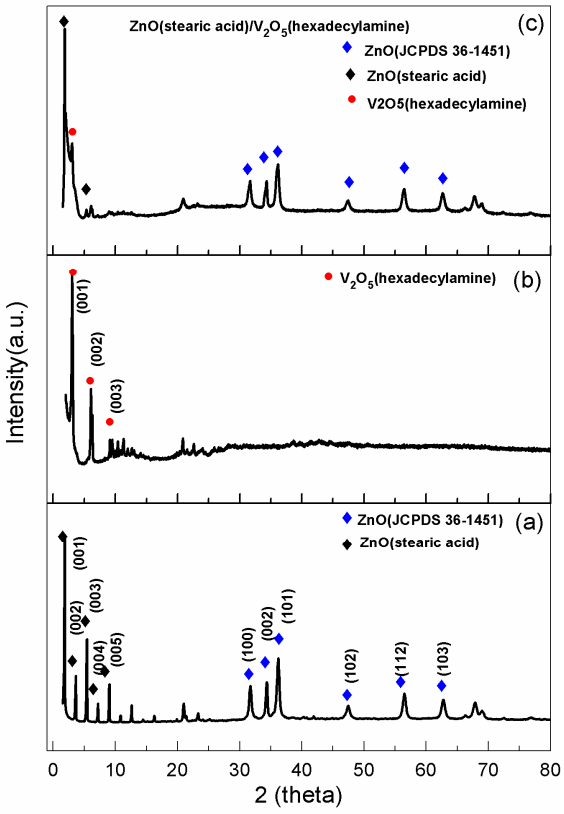

Figure 1. (a) XRD patterns of ZnO(SA) (b) XRD patterns of V_2O_5(HDA) and (c) XRD patterns of nanocomposite heterojunction ZnO(SA)/V_2O_5(HDA)

The chemical states of the ZnO(SA)/V_2O_5(HDA) composite were investigated by X-ray photoelectron spectra (XPS) as shown in Figure 2. The XPS survey spectra (Figure S1) indicate the presence of Zn, V, O and C in the surface of the composite. The deconvolution of the high resolution spectra for Zn 2p, V 2p, and O 1s are shown in the Figures 2(a-c). The binding energies for the Zn $2p_{3/2}$ and $2p_{1/2}$ core levels at 1021.6 eV and 1044.6 eV respectively in Figure 2(a), indicates the presence of ZnO in the composite. The Figure 2(b), show the V $2p_{3/2}$ spectrum of the composite, with two components centered at 516.8 eV and 515.5 eV, corresponding to the binding energies for the V^{5+} and V^{4+} species, in agreement with the presence of V_2O_5 and VO_2[39]. The O 1s spectrum (Figure 2c) contains two peaks, at 530 eV and 531 eV with characteristic binding energies for O2- oxidation state, and the peak at 531-532 eV has been assigned to the oxygen of surfactants of the composite[40].

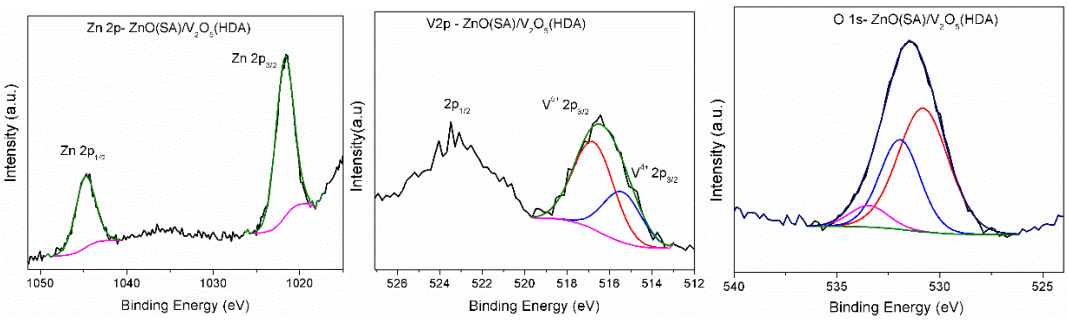

Figure 2. XPS spectra of core level (a) Zn2p, (b) V2p and (c) O1s.

Peer-reviewed version available at Catalysts 2018, 8, 374; doi:10.3390/catal8090374

Scanning electron microscopy (SEM) were performed to investigate the morphology and microstructures of nanocomposite samples. The morphology of nanocomposites are illustrated in the micrographies in Figure 3. The SEM image shows in Figure 3(a) and (b) the layered nature of ZnO(SA) and V_2O_5(HDA) while its microstructured surface, with multi-layer laminas. Figure 3(c) presents the SEM images of the representative ZnO(SA)/V_2O_5(HDA) heterojunction and EDX patterns of confirm the presence of all constituent elements in the heterojunction. No other remarkable impurities were observed. In Figure S2 SEM images of ZnO(SA)/V_2O_5(HDA) and element mappings were further performed and it can be seen clearly that Zn and V are evenly distributed, indicating the formation of hybrid nanostructure.

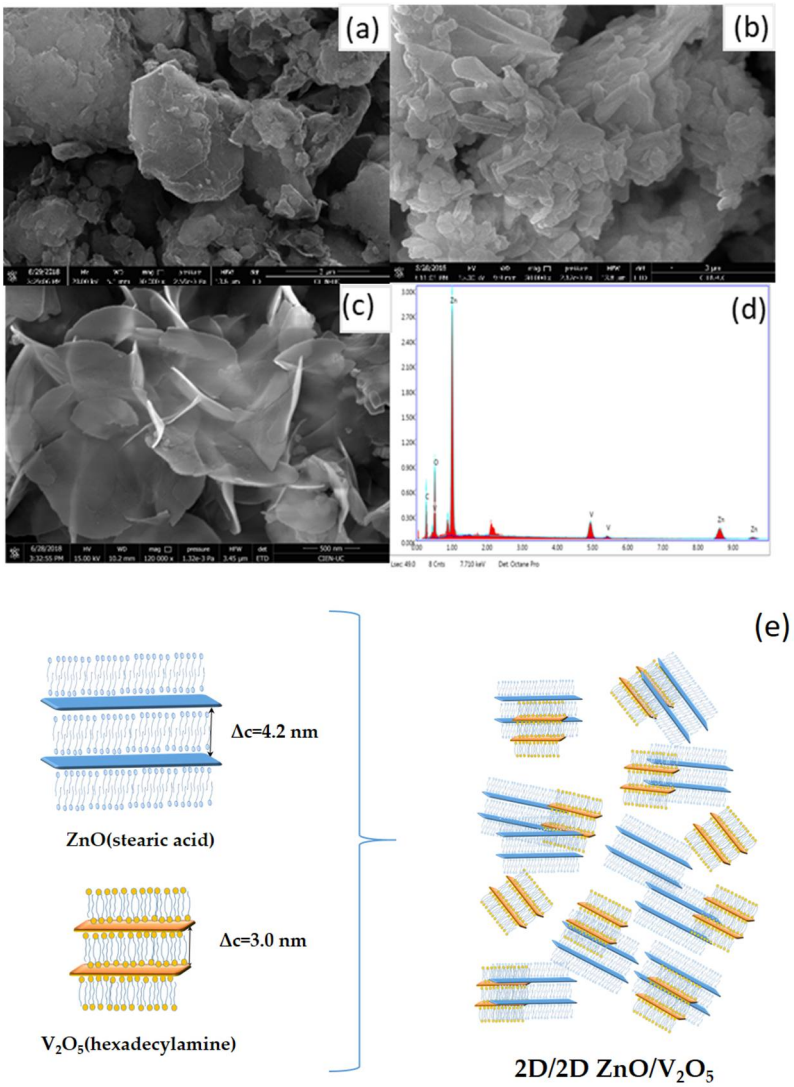

Figure 3. (a) SEM micrographs ZnO(SA) (b) SEM micrographs V_2O_5(HDA) (c) SEM micrographs ZnO(SA)/V_2O_5(HDA) (d) EDX pattern and (e) Schematic representation 2D/2D heterojunction

The UV–visible diffuse reflectance was measured for ZnO(SA), V_2O_5(HDA) and ZnO(SA)/ V_2O_5(HDA) to determine their light absorption characteristics (Figure S3). The wavelength distribution of the absorbed light is an important property of photocatalysts, irrespective of the quantum yield. Therefore, the high photoactivity were attributed to higher visible light absorbance, as indicated by UV–visible diffuse reflectance spectroscopy. The absorption bands in the range of 200–400 nm, observed in all spectra, suggest strong free exciton absorption at room temperature. The band gap of samples can be estimated from a plot of $(\alpha h\upsilon)^2$ versus the photon energy, and the intercept of a tangent to the x-axis was recorded as shown in Figure S4 were energies, Eg, determined from the spectra are 3.28 and 2.28 eV for ZnO(SA) and V_2O_5(HDA) respectively [41]. The variation of

the band gap with respect to that of ZnO(SA) is clearly seen, the absorption edge has a clear shift toward longer wavelengths.

In Figure 4(a) the infrared analysis of ZnO(SA) shows the peaks in the region 3000-2800 cm^{-1} assigned to stretching modes of the C-H bond of the methylene group, the band at 1705 cm^{-1} corroborates the presence of ν(C-O) band of the carboxylic acid in the sample and the bands at 1560 and 1315 cm^{-1} corresponding to the asymmetric and symmetric ν(C-O) modes, respectively, demonstrate that the organic moiety is found as a carboxylate mono-coordinated to the inorganic sheets [42]. In Figure 4(b) the infrared analysis of V_2O_5(HDA) shows the peaks in the region 1000 cm^{-1} are assigned to the stretching vibration of V=O, the frequencies correspond to V=O group of the vanadyl oxygen in 1011, 997 cm^{-1} and V-O-V asymmetric stretching in 737 cm^{-1} of V_2O_5. The stretching modes of the C-H bond of the methylene group at 3000-2800 cm^{-1}. The spectrum shows a shoulder at 3136 cm^{-1} attributed to the N-H vibrational stretching mode of the hexadecylamine surfactant of the nanocomposite [43]. The spectrum infrared ZnO(SA)/V_2O_5(HDA) of composite shows in Figure 4(c) characteristics bands of both components. The observation in all IR spectra of H-O-H vibrational modes in the region 3500 cm^{-1} indicates a detectable presence of remnant water molecules.

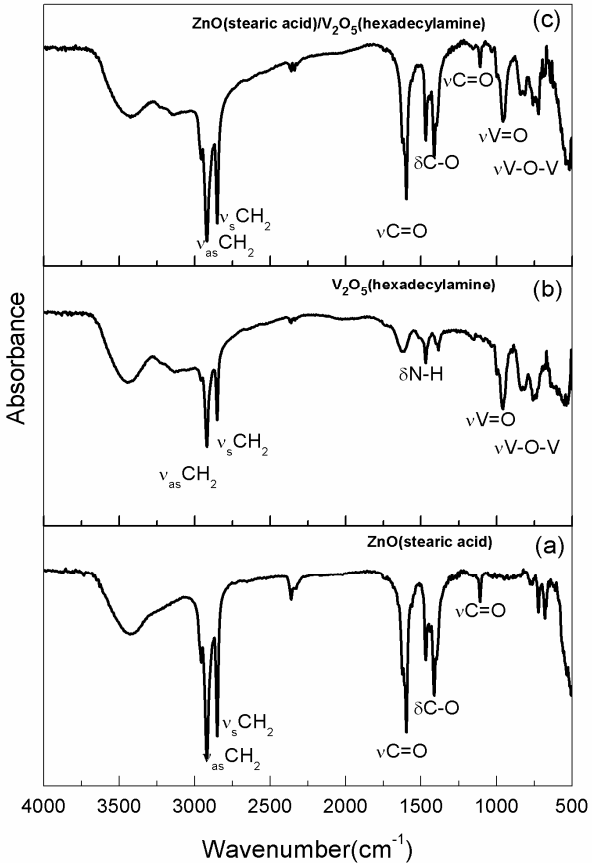

Figure 4. (a) FTIR absorbance spectra of ZnO(SA) (b) FTIR absorbance spectra of V_2O_5 (HDA) and (c) FTIR spectra of ZnO(SA)/ V_2O_5 (HDA)

Photocatalytic activity

The photocatalytic activity of nanocomposites was studied for the degradation in visible light irradiation of methylene blue as a pollutant model. To further investigate the photocatalytic behavior of hybrid ZnO/V_2O_5 molar composition were prepared by mixing the components as shown in Table S1. The V_2O_5 compounds utilized are: V_2O_5 orthorhombic, V_2O_5-xerogel and V_2O_5(HDA).

The photocatalytic properties of the as-prepared samples were evaluated under similar conditions and all curves were normalized after reaching the adsorption/desorption equilibrium (Figure S5). The results in Figure 5(a) demonstrated that the samples of heterojunctions

ZnO(SA)/V_2O_5(HDA) exhibited the highest photocatalytic efficiency in visible light irradiation. The comparison of catalytic activity of these samples indicated that 90% of the MB dye was degraded after 400 min of irradiation, the luminance of the light source was 0.5 Sun. The maximum photocatalytic activity was achieved with heterostructure hybrid ZnO(SA)/V_2O_5(HDA)1:0.25. However, the hybrid heterostructure of ZnO(SA)/V_2O_5(HDA) 1:0.5 showed lower photocatalytic ability than the other samples, which could be attributed to the higher concentration of V_2O_5 acting as a recombination center for photogenerated charge carriers and increasing the sample opacity, obstructing the light absorption and decreasing the photocatalytic activity [17]. Photocatalytic processes are very complex, and some aspects of the reaction kinetics are being studied. In this work the photocatalytic degradation of methylene blue could be described by pseudo-first-order kinetics, $\ln(C_0/C) = kt$, where k is the corresponding kinetic constant and t the irradiation time Figure 5(b). The apparent rate constants (k_{app}, min^{-1}) hybrid ZnO(SA)/V_2O_5(HDA) was about 6 time faster than for ZnO respectively. The rate constants were calculated and the linear regression coefficients (R^2) for all samples under visible light.

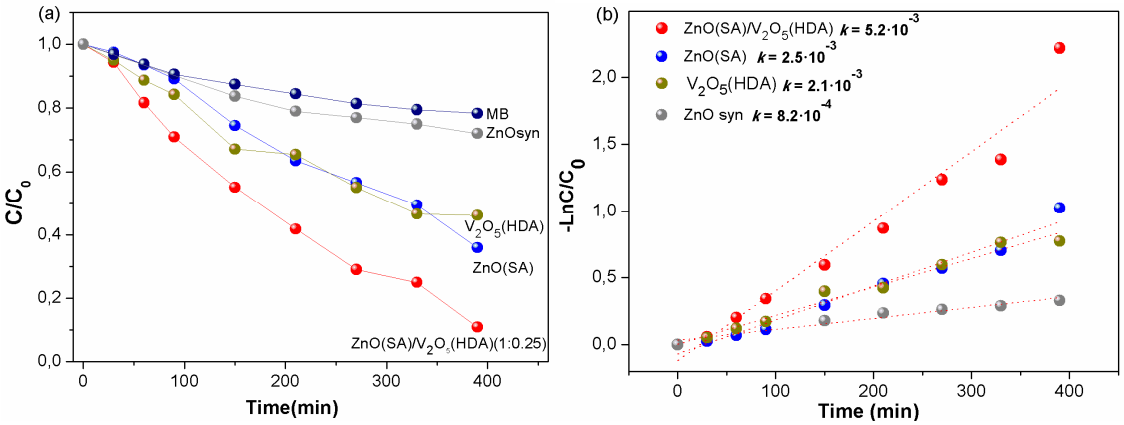

Figure 5. (a) Photocatalytic performance of the samples ZnO(SA)/ V_2O_5(HDA) for the degradation of MB solution (b) Photodegradation kinetics of the selected samples for the degradation of MB solution.

These results are in agreement qualitatively with reports on the improvement of the photocatalytic efficiency of stratified hybrid ZnO [33,37]. The shape of the MB spectrum remains unchanged throughout the process and no organic by products were detected, indicating the degradation of the dye in Figure S6. The photocatalytic performance of visible light observed indicates that there is a synergistic effect between both 2D nanocomposites used in the heterojunction, large face-to-face contact surface between the sheets, which provide more reaction sites for the adsorption of contaminants, exhibit greater stability and should lead to an interfacial charge transfer efficiency [26, 27]. In addition, the presence of an organic surfactant in the interlaminar spaces of ZnO and V_2O_5 favors the adsorption of dye on the surface of semiconductors, the abundance of hydrophobic sites for the adsorption of dye appear as probable causes of improved photocatalytic efficiency in this hybrid semiconductors heterojunction.

To further investigate the role of active species such as h^+, •OH and O_2^-• in the photocatalytic degradation of dye, the active species trapping experiments were performed using the sample ZnO(SA), V_2O_5(HDA) and ZnO(SA)/V_2O_5(HDA) 1:0.25. For these experiments, oxalate of ammonium (OA) was used as hole (h^+) scavenger (2mM), isopropanol (IPA) as a •OH scavenger (2mM) and chloroform as an O_2^-• scavenger (2mM)[44-46]. The impact of different scavengers is shown in Figure 6(a), for ZnO(SA) (64%), when the $CHCl_3$ was added into reaction solution, the photocatalytic degradation is almost invariable (60%). However, when the IPA and OA were added into solution, the degradation rate of MB inhibited (44% and 47%), respectively. Thus, the •OH and h^+ radicals are the major reactive species in the ZnO(SA) reaction. For V_2O_5(HDA) (48%), when the IPA was added

Preprints (www.preprints.org) | NOT PEER-REVIEWED | Posted: 30 July 2018 doi:10.20944/preprints201807.0583.v1

Peer-reviewed version available at Catalysts 2018, 8, 374; doi:10.3390/catal8090374

to the reaction solution photocatalytic degradation drops to 5% indicating that •OH is the major reactive species in the reaction. On the other hand, for the ZnO(SA)/V_2O_5(HDA) sample (90%), it can be seen that when the OA and IPA were added, the photocatalytic degradation rate is decreased (53% and 54%), respectively indicating the h^+ an •OH are the predominant active species. When the $CHCl_3$ was added to the reaction solution, the degradation rate of the inhibited slightly (68%), suggesting the O_2^{-}• affects less in the photocatalysis process. Thus from these experiments, we conclude •OH and h^+ as major active species in photocatalytic degradation of MB under visible light irradiation.

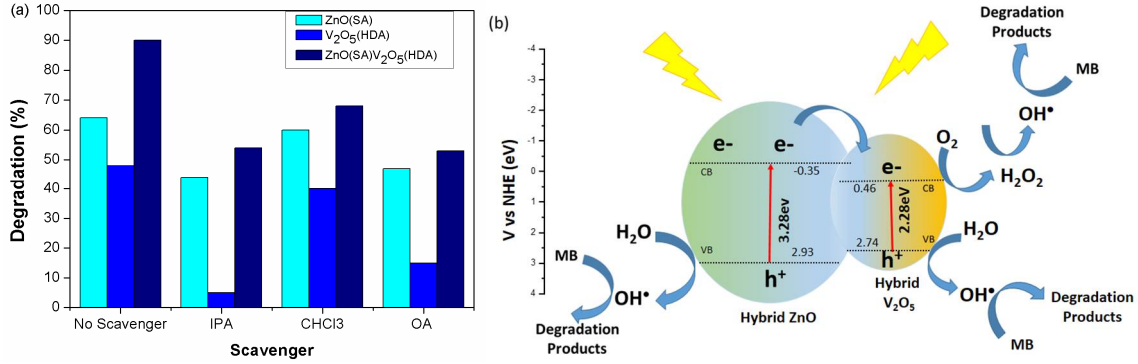

Figure 6. (a) Photocatalytic degradation of MB under visible light after addition of several trapping reagents (b) Possible mechanism of the photocatalytic activity of ZnO(SA)/V_2O_5(HDA) for degradation under visible light irradiation.

The activity of photocatalyst depends of the effective separation of electron–hole pairs and the migration of the photogenerated charge is related to the band edge position in conduction band (CB) and valence band (VB) of semiconductors. The band gap position (CB and VB) for hybrid ZnO and V_2O_5 were calculated applying the equations reported in the literature [46]:

$$E_{CB} = \chi - E^e - \tfrac{1}{2}E_g$$

$$E_{CB} = E_{VB} - E_g$$

where χ is the electronegativity of semiconductor (ZnO and V_2O_5 are 5.79 and 6.10 eV respectively); E^e is the energy of free electrons on the hydrogen scale (4.5 eV); and the band gap energy (E_g) of the semiconductor calculated from DRS data [40]. The calculated CB and VB edge positions of hybrid ZnO are -0.35 eV and 2.93 eV. As for hybrid V_2O_5, the CB and VB edge positions are 0.46 eV and 2.74 eV, respectively.

Therefore, the photon energy higher or equal to band gap energy of ZnO and V_2O_5, electrons can be excited form the VB to the CB with simultaneous generation of holes in the VB. Due to the CB of ZnO(SA) is more negative than that of the V_2O_5(HDA), electrons on the CB of ZnO(SA) can be easily injected into the CB of V_2O_5(HDA) by the interface. The photogenerated electrons on the CB of V_2O_5(HDA) could not produce O_2^{-}• from dissolved O_2 by photoreduction radicals due to the position of CB is more positive than the potential of O_2/O_2^{-}• (−0.33 V vs. NHE). However, the reduction potential of O_2/H_2O_2 is 0.695 eV vs NHE, means electrons can react with O_2 and H^+ to produce H_2O_2 which produce •OH, which is an indirect way to form the •OH [46]. Meanwhile the photoinduced holes of VB of V_2O_5 and ZnO can oxidize adsorbed H_2O molecules to produce •OH (•OH /H_2O is 2.72 eV vs NHE). •OH radicals are very reactive oxidative species to degrade of dye. As illustrated in Figure 6(b), the prepared heterojunction ZnO/V_2O_5 improve the photogenerated electron–hole pair's separation and transfer favored by extensive interface area, as well as show an oxidation and reduction ability for efficiency degradation of organic pollutants.

Stability of the photocatalyst. We have also investigated the stability and reusability of the ZnO(SA)/V_2O_5(HDA) photocatalyst over three cycles for a period of 400 min irradiation[46-47]. Figure S7 shows of loss approx. 10% in photocatalytic activity which might be due to the loss of the photocatalyst by centrifugation, washing and drying of sample, during each cycle of reusability. No significant changes in neither the dye degradation efficiency loss nor photocatalyst structure occur.

3. Materials and Methods

3.1. Materials

All the reagents in this study were commercial products purchased from Sigma-Aldrich and Merck, and were used without further purification. Nanopure water was obtained from a water purification system.

3.2. Experimental-Synthesis nanocomposites

3.2.1. Synthesis of ZnO(stearic acid)- ZnO(SA)

ZnO-stearic acid nanocomposite was synthesized as described in a previous paper [36]. In a typical procedure, $ZnSO_4$ (1 mol L^{-1}) was mixed with Na_2CO_3 (1 mol L^{-1})/ NaOH (1 mol L^{-1}) (1:1) to bear a ZnO hydrogel; then stearic acid (SA) 4.0 x 10-1 mol L^{-1} aqueous solution was added to the ZnO hydrogel solution under stirring at room temperature; the suspension was stirred at 60°C followed by an aging period of 24 h at room temperature. The sample was washed and dried at 80°C for 72 h. Analysis: % found (calculated) for $ZnO(C_{18}H_{36}O_2)_{0.38}$ x0.5H_2O, C: 41.94(41.65), H: 7.20(7.22).

3.2.2. Synthesis of compounds vanadium pentoxide

V_2O_5 xerogel, a mixture of t-butyl alcohol and orthorhombic V_2O_5 was refluxed for 6 h to form the xerogel. Water was added to the resulting dark yellow solid and the remaining t-butyl alcohol was removed with excess water under vacuum. Water was added to yield a suspension. The material was aged at room temperature yielding a red-brown colloidal V_2O_5 [37].

V_2O_5 (hexadecylamine)- V_2O_5(HDA). A solution of 10^{-3} mol of hexadecylamine (HDA) in pure ethanol, previously degassed was mixed with 2×10^{-3} mol of vanadium triisopropoxide (VOTPP) [37]. The yellow solution, obtained after vigorous stirring in an argon atmosphere for 1 h, was then hydrolyzed by adding 15 mL of water. The orange suspension obtained after stirring for 24 h. and subjected to a hydrothermal treatment in a Teflon lined autoclave at 180 °C for 6 days. From the resulting a orange solid was separated, washed with pure ethanol and water, the sample was washed and dried at 80 oC for 72 h Analysis: % found (calculated) for $V_2O_5(HDA)_{0.83}$x1.8H_2O. Anal. C: 38.32(39.06); H: 7.89(8.05); N: 2.79(2.56)

V_2O_5 orthorhombic, Aldrich.

The samples were mixed mechanically in an agate mortar (relation w/w). These samples were denoted as ZnO(SA)/V_2O_5; ZnO(SA)/ V_2O_5-xerogel and ZnO(SA)/V_2O_5(HDA).

3.3. Photocatalytic experiments

The photocatalytic activity of nanocomposites was studied for the degradation in visible light irradiation of methylene blue as a pollutant model. For this study, the characteristic absorption peak of MB at 664 nm was monitored using a Uv-vis spectrophotometer at regular intervals of time and the corresponding absorption spectra. The photocatalytic activity of the products were evaluated by measuring the degradation of methylene blue (MB) in water. The nanocomposite ZnO(SA) (10 mg) and compounds of V_2O_5 in different proportions in 25 mL of a 1 x 10^{-5} mol L^{-1} which solution phosphate buffer prepared mixing solutions of Na_2HPO_4 and NaH_2PO_4. Prior to irradiation, the suspension was magnetically stirred for 30 min, to establish an adsorption/desorption equilibrium.

The suspensions were irradiated by a 300 W Xe arc lamp (Newport) with a UVIR-CUT filter at $\lambda \geq 400$ nm, the luminance of the light source over the reactant solution was 0.5 Sun. All samples were constant magnetic stirring to ensure a higher level of homogeneity of the photocatalyst in the suspension. The MB concentration after equilibration was regarded as the initial concentration (C_0)

and was monitored in the UV–vis spectra of the solution (Perkin Elmer Lambda 35), using nanopure water as a reference.

3.4. Characterization

X-ray diffraction (XRD) analyses of the products were performed using a Bruker D8 Advance (Cu Kα λ = 1.5418 Å). The Scanning Electron Microscopy (SEM) and images were obtained by using an EVO MA 10 ZEISS microscope. X-ray photoelectron spectra (XPS) were obtained in a STAIB system with a RQ-300 X-Ray source, using monochromated Al Kα X-rays (1486.6 eV, 75 W). The charge referencing was done against adventitious carbon (C 1s 285 eV). Zn 2p, V 2p, O 1s, and C1s energy regions were scanned with several sweeps until a good signal-to-noise ratio was observed. Chemical analysis were obtained by using (SISONS ES-1108). The diffuse reflectance UV–vis spectra were recorded in the range of 200–800 nm using a Perkin Elmer Lambda 35 spectrometer. Reflectance measurements were converted to absorption spectra using the Kubelka-Munk function. Fourier transform infrared (FTIR) spectra were recorded an FT/IR-4600 Jasco spectrometer.

4. Conclusions

In summary, we have reported successfully the fabrication of the new heterojunction of two 2D hybrid layered semiconductors, ZnO/V_2O_5 exhibiting improved photocatalytic activity than the pristine zinc oxide in the degradation of methylene blue under visible light. The efficacy of the products described as catalysts for the photooxidation of organic pollutants is associated with the surface properties of 2D layered hybrid nanocomposites, collection efficiency for visible light and the presence of organic surfactant in the interlaminar spaces of ZnO and V_2O_5 favors the adsorption of the dye on the surface of semiconductors. The nanocomposites of V_2O_5 effectively inhibit the recombination of photogenerated electron/hole pairs. The products are recyclables and seen as potentially useful for environmental remediation issues.

Supplementary Materials: Supplementary material is presented

Acknowledgments: Work supported by UTEM, UCh, FONDECYT 1151189, 1171803, Basal Financing Program CONICYT, FB0807 (CEDENNA). CMST acknowledges the support from the Spanish MINECO projects PHENTOM (FIS2015-70862-P), Severo Ochoa (SEV-2013-0295) and from the CERCA Programme/Generalitat de Catalunya.

Author Contributions: Juan Aliaga and Nasla Cifuentes conceived and designed the experiments. Nasla Cifuentes performed the experiments. Eglantina Benavente, Clivia Sotomayor-Torres and Guillermo Gonzalez analyzed the data and discussed results. Juan Aliaga contributed reagents/materials/analysis tools. Eglantina Benavente and Guillermo Gonzalez wrote the paper.

Conflicts of Interest: The authors declare no conflict of interest.

References

1. Chan, S.H.; Wu, T.Y.; Juan, J.C.; The, C.Y. Recent developments of metal oxide semiconductors as photocatalysts in advanced oxidation processes (AOPs) for treatment of dye waste-water. *Chem. Technol. Biotechnol.* **2011**, *86*, 1130-1158. [10.1002/jctb.2636]
2. Ray, C.; Pal, T. Recent advances of metal–metal oxide nanocomposites and their tailored nanostructures in numerous catalytic applications. *J. Mater. Chem. A* **2017**, *5*, 9465-9487. [10.1039/C7TA02116J]
3. Lang, X.; Chen, X.; Zhao, J. Heterogeneous visible light photocatalysis for selective organic transformations. *Chem. Soc. Rev.* **2014**, 43, 473-486. [10.1039/C3CS60188A]
4. Ibhadon, A.O.; Fitzpatrick, P. Heterogeneous Photocatalysis: Recent Advances and Applications. Catalysts **2013**, 3, 189-219. [10.3390/catal3010189]
5. Hernandez, S.; Hidalgo, D.; Sacco, A.; Chiodoni, A.; Lamberti, A.; Cauda, V.; Tresso, E.; Saracco, G. Comparison of photocatalytic and transport properties of TiO_2 and ZnO nanostructures for solar-driven water splitting. *Phys. Chem. Chem. Phys.* **2015**, 17, 7775-7786. [10.1039/c4cp05857g]

6. Xia, Y.; Wang, J.; Chen, R.; Zhou, D.; Xiang, L. A Review on the Fabrication of Hierarchical ZnO Nanostructures for Photocatalysis Application. Crystals **2016**, *6*, 148. [10.3390/cryst6110148]
7. Banerjee, S.; Dionysiou, D.D.; Pillai, S.C. Self-Cleaning applications of TiO_2 by photo-induced hydrophilicity and photocatalysis. *App. Catal. B: Environmental* **2015,** *176–177*, 396-428. [10.1016/j.apcatb.2015.03.058]
8. Chen, X.; Wu, Z.; Liu, D.; Gao, Z. Preparation of ZnO photocatalyst for the efficient and rapid photocatalytic degradation of Azo dyes. *Nanoscale Res. Lett*. **2017**, *12*, 143. [10.1186/s11671-017-1904-4]
9. Lee, K.M.; Lai, C.W.; Ngai, K.S.; Juan, J.C. Recent developments of zinc oxide based photocatalyst in water treatment technology: A review. *Water Res* **2016,** *88*, 428-448. [10.1016/j.watres.2015.09.045]
10. Wang, J.; Xia, Y.; Dong, Y.; Chen, R.; Xiang, L.; Komarneni, S. Defect-rich ZnO nanosheets of high surface area as an efficient visible-light photocatalyst. *App. Catal. B: Environmental* **2016,** 192, 8-16. [10.1016/j.apcatb.2016.03.040]
11. Song, X.; Dong, D.; Yang, P. Formation of nanoplate-based clew-like ZnO mesocrystals and their photocatalysis application. *RSC Adv.* **2016**, 6, 51544-51551. [10.1039/C6RA07874E]
12. Fageria, P.; Gangopadhyay, S.; Pande, S. Synthesis of ZnO/Au and ZnO/Ag nanoparticles and their photocatalytic application using UV and visible light. *RSC. Adv*. **2014**, *4*, 24962-24972.[10.1039/C4RA03158J]
13. Zhang, Y.; Xu, J.; Xu, P.; Zhu, Y.; Chen, X.; Yu, W. Decoration of ZnO nanowires with Pt nanoparticles and their improved gas sensing and photocatalytic performance. *Nanotechnology* **2010**, *21*, 285501-285508. [10.1088/0957-4484/21/28/285501]
14. Mendoza-Mendoza, E.; Nuñez-Briones, A.G.; García-Cerda, L.A.; Peralta-Rodríguez, R.D.; Montes-Luna, A.J. One-step synthesis of ZnO and Ag/ZnO heterostructures and their photocatalytic activity. *Ceram. Int.* **2018**, *44*, 6176-6180.[10.1016/j.ceramint.2018.01.001]
15. Mani, J.; Sakeek, H.; Habouti, S.; Dietze, M.; Es-Souni, M. Macro–meso-porous TiO_2, ZnO and ZnO-TiO_2 composite thick films. Properties and application to photocatalysis. *Catal. Sci. Technol*, **2012**, *2*, 379-385. [10.1039/C1CY00302J]
16. Balachandran, S.; Prakash, N.; Thirumalai, K.; Muruganandham, M.; Sillanpää, M.; Swaminathan, M. Facile construction of heterostructured $BiVO_4$–ZnO and its dual application of greater solar photocatalytic activity and self-cleaning property. *Ind. Eng. Chem. Res.* **2014,** 53, 8346–8356. [10.1021/ie404287m]
17. Sun, C.; Fu, Y.; Wang, Q.; Xing, L.; Liu, B.; Xue, X. Ultrafast piezo-photocatalytic degradation of organic pollutions by Ag2O/tetrapod-ZnO nanostructures under ultrasonic/UV exposure. *RSC Adv*. **2016**, *6* 87446-87453. [10.1039/C6RA13464E]
18. Kandjani, K.; Sabri, Y.; Periasamy, S.; Zohora, N.; Amin, M.; Nafady, A.; Bhargava, S. Controlling core/shell formation of nanocubic p-Cu2O/n-ZnO toward enhanced photocatalytic performance. *Langmuir* **2015**, 39, 10922–10930. [10.1021/acs.langmuir.5b01019]
19. Vikas, L.S.; Vanaja, K.A.; Subha, P.P.; Jayaraj, M.K. Fast UV sensing properties of n-ZnO nanorods/p-GaN heterojunction. *Sensors and Actuators A* **2016**, *242*, 116–122. [10.1016/j.sna.2016.02.038]
20. Adhikari, S.; Sarkar, D.; Madras, G. Highly efficient WO_3–ZnO mixed oxides for photocatalysis. *RSC Adv.* **2015**, *5*, 11895-11904. [10.1039/C4RA13210F]
21. Ahmeda, L.T.; Ma, M.; Edvinsson, T.; Zhua, J. A facile approach to ZnO/CdS nanoarrays and their photocatalytic and photoelectrochemical properties. *App. Catal. B: Environmental* **2013,** *138–139*, 175-183. [10.1016/j.apcatb.2013.02.042]
22. Zaera, F. New challenges in heterogeneous catalysis for the 21st century. *Catal. Lett.* **2012**, *142*, 501-516. [10.1007/s10562-012-0801-9]
23. Ebrahimi, M.; Samadi, M.; Yousefzadeh, S.; Soltani, M.; Rahimi, A.; Chou,T.; Chen, L.; Chen, K.; Moshfegh, A. Improved solar-driven photocatalytic activity of hybrid graphene quantum dots/ZnO nanowires: A direct Z-scheme mechanism. *ACS Sustainable Chem. Eng*. **2017**, *5*, 367–375. [10.1021/acssuschemeng.6b01738]
24. Colombo, E.; Li, W.; Bhangu, S.; Ashokkumar, M. Chitosan microspheres as a template for TiO_2 and ZnO microparticles: studies on mechanism, functionalization and applications in photocatalysis and H_2S removal. *RSC Adv.* **2017**, 7**,** 19373-19383. [10.1039/C7RA01227F]
25. Anastasio, P.; Del Giacco, T.; Germani, R.; Spretic, N.; Tiecco, M. Structure effects of amphiphilic and non-amphiphilic quaternary ammonium salts on photodegradation of Alizarin Red-S catalysed by titanium dioxide. *RSC Adv.* **2017** , *7*, 361-368. [10.1039/C6RA25421G]

26. Low, J.; Cao, S.; Yu, J.; Wageh. S. Two-dimensional layered composite photocatalysts. Chem. Commun. **2014**, *50*, 10768-10777. [10.1039/C4CC02553A]
27. Li, Y.; Li, Y.L.; Sa, B.; Ahujad, R. Review of two-dimensional materials for photocatalytic water splitting from a theoretical perspective. *Catal. Sci. Technol*., **2017**, *7*, 545-559. [10.1039/C6CY02178F]
28. Zhang, Z.; Huang, J.; Zhang, M.; Yuan, Q.; Dong, B. Ultrathin hexagonal SnS2 nanosheets coupled with g-C3N4 nanosheets as 2D/2D heterojunction photocatalysts toward high photocatalytic activity. *App. Catal., B* **2015**, 163, 298–305. [10.1016/j.apcatb.2014.08.013]
29. Yuan, C.; Hung, C.; Yuan, C.; Wen. H. Preparation and application of immobilized surfactant-modified PANi-CNT/TiO_2 under visible-light irradiation. *Materials* **2017**, 10, 877-897. [10.3390/ma10080877]
30. Zhu, X.; Yuan, C.; Chen. C. Photocatalytic degradation of pesticide pyridaben. 3. In surfactant/TiO_2 aqueous dispersions. *Environ. Sci. Technol.* **2007**, *41*, 263-269. [10.1021/es061178+]
31. Duta, M.; Perniu, D.; Duta, A. Photocatalytic zinc oxide thin films obtained by surfactant assisted spray pyrolysis deposition. *App. Surf. Sci.* **2014**, *306*, 80–88. [10.1016/j.apsusc.2014.02.132]
32. Hao, C.; Wang, J.; Cheng, Q.; Bai, Y.; Wang, X.; Yang,Y. Anionic surfactants-assisted solution-phase synthesis of ZnO with improved photocatalytic performance. *J Photochem. Photobiol A: Chem*. **2017**, *332*, 384-390. [10.1016/j.jphotochem.2016.09.013]
33. Benavente, E.; Navas, D.; Devis, S.; Segovia, M.; Sotomayor-Torres, C.; González, G. Composites of laminar nanostructured ZnO and VOx-Nanotubes hybrid as visible light active photocatalysts. Catalysts **2018**, 8, 93. [10.3390/catal8020093]
34. Yin, H.; Yu, K.; Hu, J.; Song, C.; Guo, B.; Wang, Z.; Zhu, Z. Novel photoluminescence properties and enhanced photocatalytic activities for V2O5-loaded ZnO nanorods. *Dalton Trans*. *2015*, **10**, 4671-4678. [10.1039/c5dt00015g]
35. Zou, C.W.; Rao, Y.F.; Alyamani, A.; Chu, W.; Chen, M.J.; Patterson, D.A.; Emanuelsson, E.A.; Gao, W. Heterogeneous lollipop-like V_2O_5/ZnO Array: A promising composite nanostructure for visible light photocatalysis. *Langmuir* **2010,** *14*, 11615–1162. [10.1021/la101324e]
36. Aslam, M.; Ismail, I.; Almeelbi, T.; Salah, N.; Chandrasekaran, S.; Hameed, A. Enhanced photocatalytic activity of V_2O_5–ZnO composites for the mineralization of nitrophenols. *Chemosphere* **2014,** *117*, 115–123. [10.1016/j.chemosphere.2014.05.076]
37. Segovia, M.; Lemus, K.; Moreno, M.; Santa Ana, M.A.; González, G.; Ballesteros, B.; Sotomayor C.; E. Benavente. Zinc oxide/carboxylic acid lamellar structures. *Mater. Res. Bull*. **2011**, *46*, 2191–2195. [10.1016/j.materresbull.2011.06.040]
38. O'Dwyer, C.; Navas, D.; Lavayen, V.; Benavente, E.; Santa Ana, M.A.; González, G.; Newcomb, S:B.; Sotomayor Torres, C.M. Nano-Urchin: The formation and structure of high-density spherical clusters of vanadium oxide nanotubes. *Chem. Mater*. **2006**, *13*, 3016-3022. [10.1021/cm0603809]
39. Asim, N.; Radiman, S.; Yarmo, M.A. Preparation and characterization of core–shell polyaniline/V_2O_5 nanocomposite via microemulsion method. *Mater. Lett.* **2008,** *62*, 1044-1047. [10.1016/j.matlet.2007.07.051]
40. Martha, S.; Das, D.P.; Biswal, N.; Parida, K.M. Facile synthesis of visible light responsive V_2O_5/N,S–TiO_2 composite photocatalyst: enhanced hydrogen production and phenol degradation. *J. Mater. Chem*. **2012,** *22*, 10695-10703. [10.1039/C2JM30462G]
41. Xu, Y.; Schoonen, M. The absolute energy positions of conduction and valence bands of selected semiconducting minerals. *Am. Mineral*. **2000**, *85*, 543–556. [10.2138/am-2000-0416]
42. Mendive, C.B.; Bahnemann, D.W.; Blesa, M.A. Microscopic characterization of the photocatalytic oxidation of oxalic acid adsorbed onto TiO_2 by FTIR-ATR. *Catalysis Today* **2005**, 237–244. [10.1016/j.cattod.2005.03.016]
43. O'Dwyer, C.; Lavayen, V.; Newcomb, S.B.; Santa Ana, M.A.; Benavente, E.; González G.; Sotomayor-Torres, C.M. Vanadate conformation variations in vanadium pentoxide nanostructures. *J. Electrochem. Soc*. **2007**, *154*, K29-K35. [10.1149/1.2746556]
44. Liu, H.R.; Shao, G.X.; Zhao, J.F.; Zhang, Z.X.; Zhang, Y.; Liang, J.; Liu, X.G.; Jia, H.S.; Xu, B.S. Worm-like Ag/ZnO core-shell heterostructural composites: fabrication, characterization, and photocatalysis. *J. Phys. Chem. C* **2012**, *116*, 16182-16190. [10.1021/jp2115143]
45. Kumar, S.; Sharma, V.; Bhattacharyya, K.; Krishnana, V. N-doped ZnO-MoS_2 binary heterojunctions: Dual role of 2D MoS2 in the enhancement of photostability and photocatalytic activity under visible light irradiation for tetracycline degradation. *Mater. Chem. Front.* **2017**,*1*, 1093-1106. [10.1039/C6QM00274A]

46. Hong, Y.; Jiang Y.; Li, C., Fan W.; Yan, X.; Yan M.; Shi, W. In-situ synthesis of direct solid-state Z-scheme V_2O_5/g-C_3N_4 heterojunctions with enhanced visible light efficiency in photocatalytic degradation of pollutants. *Appl. Catal., B.* **2016**, *180,* 663–673. [10.1016/j.apcatb.2015.06.057]
47. Dong, F.; Sun, Y.; Fu. M. Enhanced visible light photocatalytic activity of V_2O_5 cluster modified N-Doped TiO_2 for degradation of toluene in air. *Int. J. Photoenergy*. **2012**, 10, 569716. [10.1155/2012/569716]